Progress In Electromagnetics Research, Vol. 138, 453–466, 2013

INVESTIGATION OF QUASI-OPTICAL BESSEL-GAUSS RESONATOR AT MM- AND SUBMM-WAVELENGTHS

Yanzhong Yu[1, 2, *] and Wenbin Dou[2]

[1]College of Physics & Information Engineering, Quanzhou Normal University, Quanzhou 362000, China

[2]State Key Lab of Millimeter Waves, Southeast University, Nanjing 210096, China

Abstract—A research of a quasi-optical Bessel-Gauss resonator (QOBGR) at millimeter (MM) and submillimeter (SubMM) wavebands is presented in this paper. The design is based on the quasi-optical theory and technique. The iterative Stratton-Chu formula (ISCF) algorithm is employed to analyze the output characteristics of the cavity, including the resonant modes, phases, power losses and phase shifts. Analysis of the results demonstrates that the present design of the QOBGR can support zero order or any high order mode of the pseudo Bessel-Gauss beam. At the output plane the intensity distributions of these modes are modulated by a Gauss-shaped envelope, and their phase patterns have an approximate block-like profile. Tolerance analysis for the designed QOBGR is also done. Lastly, a comparison of resonating modes is made between QOBR (quasi-optical Bessel resonator) and QOBGR when both are configured with the same geometric parameters.

1. INTRODUCTION

Bessel beams are a family of ideal nondiffracting beams, which are discovered and presented in the seminal work of Durnin and coworkers in 1987 [1, 2]. It is known that an ideal Bessel beam would have an infinite bound in the cross-section and possess an infinite amount of energy. Consequently, a true Bessel beam cannot be generated physically [3]. In order to overcome the difficulties in practically producing Bessel beams, the transformative beams, i.e., Bessel-Gauss beams were thus brought forward [4, 5]. These types of

Received 20 February 2013, Accepted 27 March 2013, Scheduled 30 March 2013

* Corresponding author: Yanzhong Yu (yuyanzhong059368@gmail.com).

beams are modulated by the Gaussian functions, and therefore they extend finitely in the radial direction and carry a limited amount of energy. It has been demonstrated that the Bessel-Gauss beams are approximations to diffraction-free beams [6]. Bessel-Gauss beams have many potentials applications and have attracted much attention [7–11]. How to generate effectively Bessel-Gauss beams is an important subject that is worth studying. Several different methods in optics have been proposed to generate the Bessel-Gauss beams [6, 12–16]. To our knowledge, no method has yet been proposed to generate these beams at mm- and sub mm-wavelengths. Therefore, a QOBGR supporting Bessel-Gauss modes at these wavebands is designed and analyzed for the first time in the present paper. A design of QOBGR is based on quasi-optical techniques, and an analysis of its output characteristics is done by employing the ISCF method, which is developed and validated in our previous paper [17]. We also carry out the research of tolerance analysis for the designed QOBGR. Finally, the output properties of QOBGR are compared with those of QOBR.

The rest of the present paper is organized as follows. An introduction of Bessel-Gauss beams is described in Section 2. The QOBGR is designed in Section 3. Section 4 presents the analysis results of the designed QOBGR, covering resonating modes in Subsection 4.1, tolerance analysis in Subsection 4.2, and a comparison between QOBGR and QOBR in Subsection 4.3. We give a brief summary in the last Section 5.

2. BESSEL-GAUSS BEAM

In the circular cylindrical coordinates system, the wavefield distribution of the ideal Bessel beam of order n is given by [1, 2]

$$E_{\mathrm{BB}}(\rho, \varphi, z) = E_0 J_n(k_\perp \rho) \exp(ik_z z) \exp(in\varphi) \tag{1}$$

where the subscript BB identifies the Bessel beam. E_0 is an amplitude constant, J_n the nth-order Bessel function of the first kind, λ a wavelength in the free space, and $\rho^2 = x^2 + y^2$, $k_\perp$ and k_z denote the transverse and longitudinal wavevectors, with $k = \sqrt{k_\perp^2 + k_z^2} = 2\pi/\lambda$. The intensity distribution for a true Bessel beam obeys

$$I_{\mathrm{BB}}(\rho, \varphi, z \geq 0) = I_{\mathrm{BB}}(\rho, \varphi, z = 0) = |E_0 J_n(k_\perp \rho)|^2 \tag{2}$$

This indicates that the intensity distribution does not alter in the radial plane when this type of beam propagates along the z direction. Such beam therefore may be viewed as a nondiffracting or diffraction-free beam. Owing to the characteristic of infinite oscillation of Bessel function, an ideal Bessel beam is boundless in the transverse plane. An

infinite amount of energy should be required practically to generate such beam.

The concept of Bessel-Gauss beam was first proposed by Gori and co-workers in 1987 [4]. It has been proved that Bessel-Gauss beam is the solution to Helmholtz equation within the paraxial approximation [4, 5]. A nth-order Bessel-Gauss beam can be described in the form [6, 16, 18]

$$E_{\mathrm{BGB}}(\rho,\varphi,z) = E_0\frac{w_0}{w(z)}J_n\left(\frac{k_\perp\rho}{1+iz/z_R}\right)\exp\left\{-\left[\frac{1}{w^2(z)}-\frac{ik}{2R_g(z)}\right]\times\left(\rho^2+z^2k_\perp^2/k^2\right)\right\}\exp(i\Phi(z))\exp(in\varphi) \quad (3)$$

where the subscript BGB identifies the Bessel-Gauss beam. $w(z) = w_0[1+(z/z_R)^2]^{1/2}$ describes the axial evolution of the $1/e^2$ half-width of the Gaussian beam [19–21], and w_0 denotes the Gaussian $1/e^2$ radius at the waist (assuming the waist located at $z = 0$). $R_g(z) = z + z_R^2/z$ represents the radius of curvature of Gaussian wave front, and $z_R = kw_0^2/2$ is its Rayleigh range. $\Phi(z) = (k - k_\perp^2/2k)z - \arctan(z/z_R)$ denotes the axial phase of the Bessel-Gauss beam.

One can easily obtain the field distribution of the nth-order Bessel-Gauss beam at the waist (i.e., $z = 0$) from Eq. (3)

$$E_{\mathrm{BGB}}(\rho,\phi,z=0) = E_0J_n(k_\perp\rho)\exp\left(-\frac{\rho^2}{w_0^2}\right)\exp(in\phi) \quad (4)$$

We can find from Eq. (4) that at the waist a Gaussian modulation had been added on the Bessel beam of order n. Because of the fast

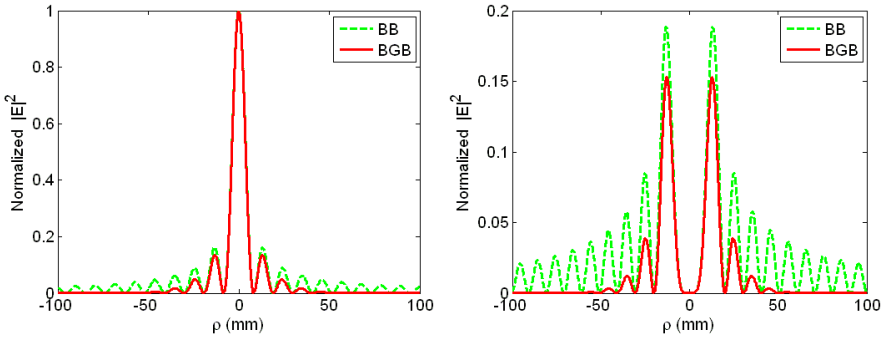

(a) zero order (b) third order

Figure 1. The normalized intensity distributions for Bessel-Gauss beam (solid line —) at the waist and Bessel beam (dash line ----). (a) zero order, and (b) high order. The relevant parameters are $\lambda = 3\,\mathrm{mm}$, $w_0 = 40\,\mathrm{mm}$, $k_\perp = 0.319\,\mathrm{mm}^{-1}$, and $\rho = 100\,\mathrm{mm}$.

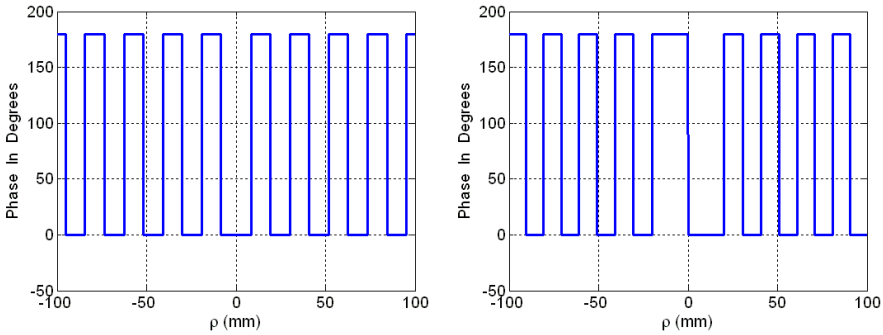

(a) zero order (b) third order

Figure 2. The phase patterns for Bessel-Gauss beam at the waist, (a) zero order, and (b) high order. All parameters are the same as in Fig. 1.

attenuation characteristic of Gaussian function, this field does not extend infinitely in the lateral plane and thus can not carry an infinite amount of energy. As illustrated in Fig. 1, not only the zero-order but also high-order Bessel-Gauss beams (solid line) oscillate limitedly along the radial direction, when compared with the ideal Bessel beams (dash line). Therefore in practice, the Bessel-Gauss beam is much easier to generate physically than Bessel beam. Fig. 2 depicts the phase distributions of Bessel-Gauss beams. It can be observed from Fig. 2 that the phase distribution of zero order is even-symmetric but the high order's is odd-symmetric about the central axis, however, both are block-shaped profiles.

3. DESIGN OF QOBGR

On the basis of quasi-optical theory and technique, a QOBGR is designed. If we want to obtain some field that we need, we can construct a cavity with end mirrors that conjugate the radial phase of this field [18]. For example, a resonator made by spherical mirrors supports a Gaussian beam, owing to its spherical wavefronts; and since a Bessel beam has conical wavefronts, an axicon (conical mirror) can be employed to form a cavity that sustains Bessel-type modes [13, 22]. By analogy, a resonator that is composed of an axicon and a spherical mirror is expected to support Bessel-Gauss modes.

As illustrated in Fig. 3(a), the configuration of the QOBGR consists of a refractive axicon, with apex angle β and refractive index η, and a concave-spherical output mirror separated a distance L. The high reflection of base plane of the refractive axicon is required,

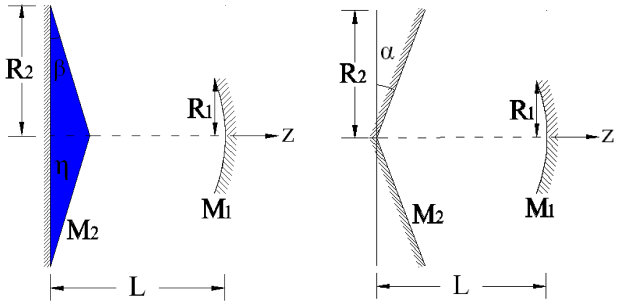

Figure 3. Configuration of the QOBGR with (a) refractive and (b) reflective axicon. The concave-spherical mirror M_1 is placed at a distance L from the axicon M_2.

however, the concave-spherical output mirror is fabricated to be only the partially reflective and therefore the resonating modes in the cavity can be outputted from it. Actually, to satisfy the requirement that the resonator may stand higher power, we can replace the refractive axicon with a reflective one that has conical angle α, as shown in Fig. 3(b). Under this equivalent case, the conical angel α is related to the apex angle β and refractive index η by: $\alpha = \arcsin(\eta \sin(\beta)) - \beta$. For the foregoing reasons, the reflective type resonator shown in Fig. 3(b) is selected to construct the Bessel-Gauss resonator in our paper. The cavity length L between the axicon M_2 and the mirror M_1 is determined by [14, 22, 23]

$$L = \frac{R_2}{2\tan\alpha} \tag{5}$$

where R_2 is the aperture radius of the refractive or reflective axicon and $R_2 = 2R_1$.

4. SIMULATION ANALYSES

4.1. Resonating Modes

It is well known that in optics the classical Fox-Li iterative algorithm [24] is quite competent to calculate the field distributions in optical cavity. It employs the scalar form of the Kirchhoff formula for diffraction to analyze the resonating modes and therefore is appropriate for the analysis of the cavity at light wavebands. Unfortunately, it is not suitable for analyzing the resonator in MM- and SubMM-range, because in optics the f-number of the cavity is always very large, and therefore the feature sizes of the cavity are usually much larger

than a light wavelength. This means the condition for using Fox-Li iterative algorithm is satisfied, and it thus can be reliably employed to analyze the resonator. However, at MM- and SubMM-range, it is impossible to design a resonator with big f-number, or the volume and weight of cavity will be unbearable. Generally, the feature sizes of cavity are on the order of MM-wavelength, and the assumptions of typical scalar-based iterative method are violated in this feature size regime. In order to calculate precisely the field behavior in the designed cavity at MM- and SubMM-wavebands, an iterative algorithm, i.e., iterative Stratton-Chu formula (ISCF) method has been developed and its validity has been demonstrated in our previous work [17]. The ISCF method is analogous to the famous Fox-Li algorithm, but it applies the vector form of the Stratton-Chu formula for diffraction [25] to calculate precisely the electromagnetic field distributions in the cavity. So, in the present paper, we still employ the ISFC method to analyze the designed QOBGR in our spectrum. Since the principle and practical implementation of this algorithm are well described in literature [17], they will not be depicted herein.

According to the configuration of cavity given in Section 3, we can form a reflective-type QOBGR readily. The relevant parameters of the designed resonator are as follows: $R_2 = 160\,\text{mm}$, $\alpha = 16^\circ$, the operating wavelength of the resonator is $\lambda = 8\,\text{mm}$, the curvature radius of the concave-spherical mirror is $K = 4184.9\,\text{mm}$. Then the aperture radius of the concave-spherical mirror is obtained by $R_1 = R_2/2 = 80\,\text{mm}$ and the value for the cavity length is calculated by Eq. (5), yielding $L = 279\,\text{mm}$.

Supposing that an initial excitation of a uniform plane wave exists on the aperture of the concave-spherical mirror, then utilizing the ISCF algorithm and after three hundred transits, the electromagnetic field distributions in the cavity reach the steady stage. At this moment, the output beam from the mirror surface can be obtained. Figs. 4(a) and (b) illustrate the transverse intensity and phase distributions of the dominant mode of the cavity, respectively. When compared with Figs. 1(a) and 2(a), we find that the output beam is an approximation to zero-order Bessel-Gauss beam, known as the pseudo Bessel-Gauss beam. By observing Fig. 4(a), one can find readily that the maximum normalized intensity of the fundamental mode is situated at the center of the concave-spherical mirror; and its intensity distribution forms an envelope with Gaussian shape (dash black line --). Indeed, the envelope curve is the intensity distribution of the lowest-order Gaussian mode. It can be obtained from a Gaussian resonator made by the concave-spherical mirror M_1 with aperture radius R_1 and a plane mirror of $R_2 = 2R_1$ separated by length L. It can be seen obviously

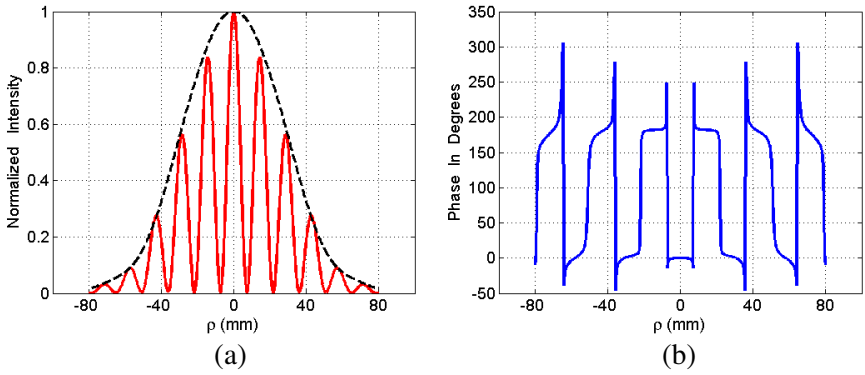

Figure 4. Transverse profiles of the intensity and phase of the fundamental Bessel-Gauss mode at the concave-spherical mirror for the designed QOBGR. (a) The intensity distribution, and (b) the phase distribution. The parameters used in Fig. 4 are: $R_1 = 80\,\text{mm}$, $R_2 = 160\,\text{mm}$, $L = 279\,\text{mm}$, $\alpha = 16°$, $K = 4184.9\,\text{mm}$, $\lambda = 8\,\text{mm}$.

from Fig. 4(b) that the phase pattern exhibits not a pure block-shaped profile but a little aberration, due to diffraction on the brink of the aperture of the concave-spherical mirror. Additionally, according to Eqs. (10) and (11) presented in article [17], the values of the power loss and phase shift per round-trip can be obtained, yielding $\delta = 0.1324\%$ and $\Phi = 1.624°$, respectively.

To achieve the high-order Bessel-Gauss mode, an excitation source of a uniform plane wave, which is not even symmetry but odd symmetry about the central axis z, is required on the concave-spherical mirror. Similarly, after three hundred transits one can get the steady state resonating modes, as shown in Fig. 5. It is easy to discover from Fig. 5(a) that the intensity profile is also a Gaussian envelope (dash black line --). However, unlike the zero-order Bessel-Gauss beam, the intensity value of high-order one is not the maximum but zero in the middle of the output mirror, owing to the existence of a phase singularity therein. Likewise, we can see from Fig. 5(b) that the phase pattern of the high-order mode still displays a block-like outline. However, the symmetry of phase pattern of high-order mode is different from that of zero-order one. The former is odd-symmetric about the central axis z but the latter is even-symmetric. The value of the power loss and phase shift per round-trip for high-order mode can be similarly obtained, i.e., $\delta = 0.9074\%$ and $\Phi = 3.5907°$, respectively. As expected, these values are larger than those of the zero-order mode, correspondingly. By observing carefully, we find that the loss in the higher order mode is almost 7 times higher and phase shift is almost twice as compared to the fundamental mode. We consider the main

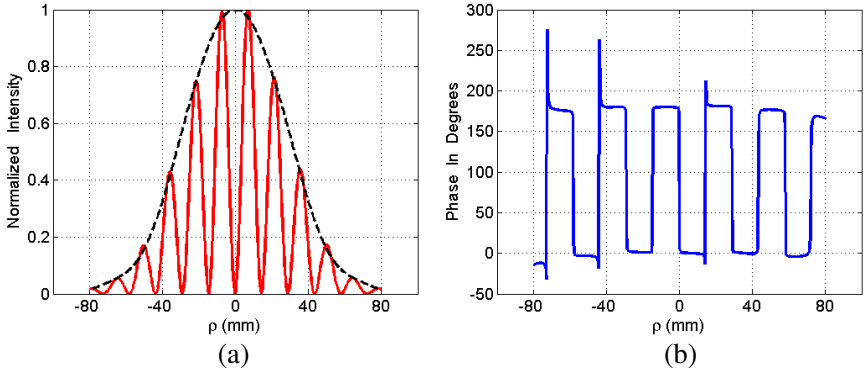

Figure 5. The transverse intensity and phase distributions of the high-order Bessel-Gauss mode at the concave-spherical mirror for the designed cavity. (a) The intensity distribution, and (b) the phase pattern. The relevant parameters are the same as in Fig. 4.

reason is that the intensity distribution of higher order Bessel-Gauss beam is null at the center of the output element, thus more power loss occur here.

4.2. Tolerance Analysis

Since the machining errors of the designed QOBGR will be hard to avoid, the tolerance analysis is very necessary. We investigate the effects of manufacture errors upon the output beams, covering their intensity and phase patterns, power loss and phase shift per round-trip. Let us assume that there are only errors in the aperture radii of reflective axicon and concave mirror, that is, $R_1 = 80 \pm 1\,\mathrm{mm}$

Table 1. The power losses and phase shifts in the aberrated cavities.

Aperture radius R_1 (mm)	Conical angle α (∘)	Cavity length L (mm)	power loss δ (%)	phase shift Φ (∘)
80	16	279	0.1324	1.6240
$80-1$	16	279	0.0489	1.5474
$80+1$	16	279	0.1612	1.6666
80	$16-0.5$	279	1.4870	60.8318
80	$16+0.5$	279	1.5118	59.9321
80	16	$279-2$	0.1076	1.3629
80	16	$279+2$	0.1465	1.6032

and $R_2 = 160 \pm 2\,\text{mm}$. Under these cases the dominant modes in the distorted cavities are calculated, respectively. Fig. 6 shows their intensity and phase profiles at the concave mirror plane. Next, the influences of the conical angle errors of $\alpha = 16 \pm 0.5°$ on the output properties are evaluated, as depicted in Fig. 7. In the same way, Fig. 8 illustrates the effects of the cavity length errors of $L = 279 \pm 2\,\text{mm}$ on the output beams. It can be observed distinctly from Figs. 6, 7 and 8 that the aberrated cavities may still well support the Bessel-Gauss modes, although there exist different machining errors. Other output characteristics, such as power losses and phase shifts, are summarized in Table 1. By observing Table 1 carefully, one may find that the power losses are close to the value of 0.1324%; however, the output characteristics are more sensitive to conical angle errors than other errors. From the Eq. (4) and Fig. 4(b), we can obtain the relation of

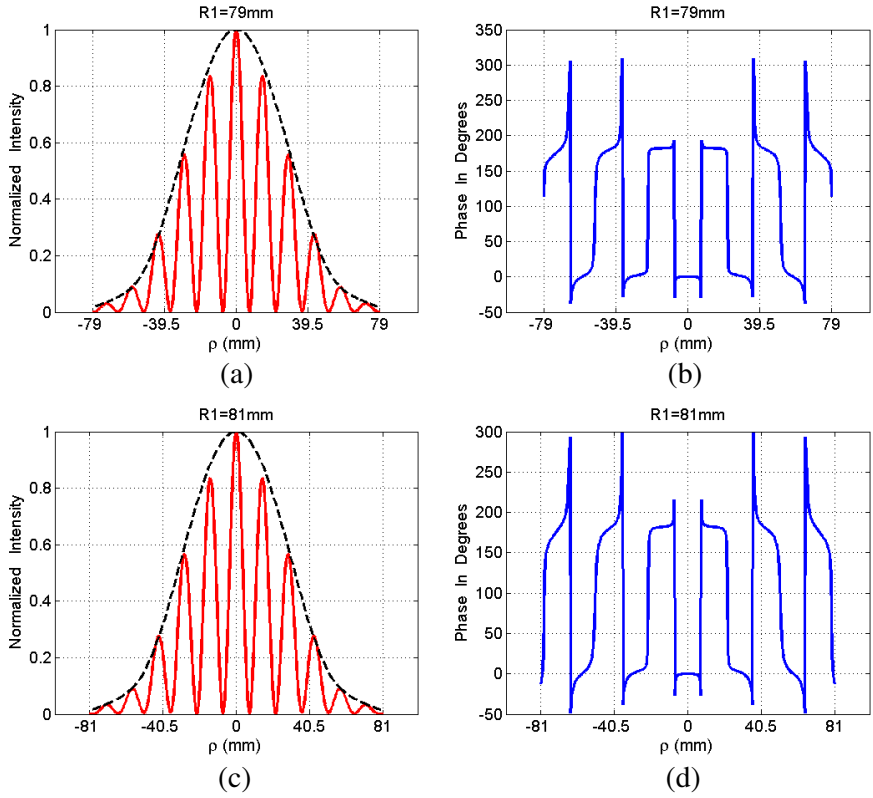

Figure 6. The effects of aperture errors on the output distributions. The intensity and phase distributions of the fundamental mode for (a), (b) $R_1 = 79\,\text{mm}$ and (c), (d) $R_1 = 81\,\text{mm}$.

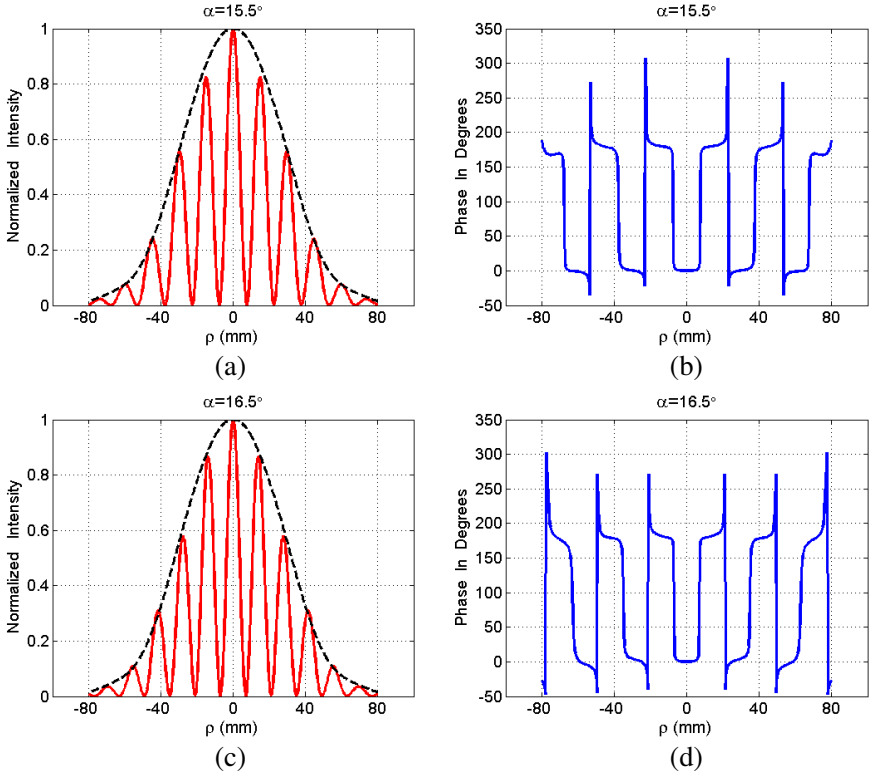

Figure 7. The influences of conical angle errors on the output beams. The intensity and phase distributions for (a), (b) $\alpha = 15.5°$ and (c), (d) $\alpha = 16.5°$.

$J_n(k_\perp \rho) = J_n(k \sin \alpha \rho)$. It can be seen that the Bessel-Gauss beam is determined directly by the conical angle α. As a results, a small error in the conical angle α can cause a strong effect on the loss and phase shift.

4.3. Comparison between QOBR and QOBGR

At last, a comparison of resonating modes is made between QOBR and QOBGR when both cavities have the same geometric parameters, i.e., $R_2 = 6\,\text{mm}$, $R_1 = 3\,\text{mm}$, $\alpha = 20°$, $L = 8.2\,\text{mm}$, and $\lambda = 0.6\,\text{mm}$. However, it is worth mentioning that the mirror M_1 for the QOBGR is a concave mirror with a curvature radius of $K = 74.2\,\text{mm}$, but for the QOBGR it becomes a plane. The radial intensity distributions of the fundamental and high-order modes for two resonators are displayed in Figs. 9(a) and (b), respectively. It can be found from Fig. 9 that near

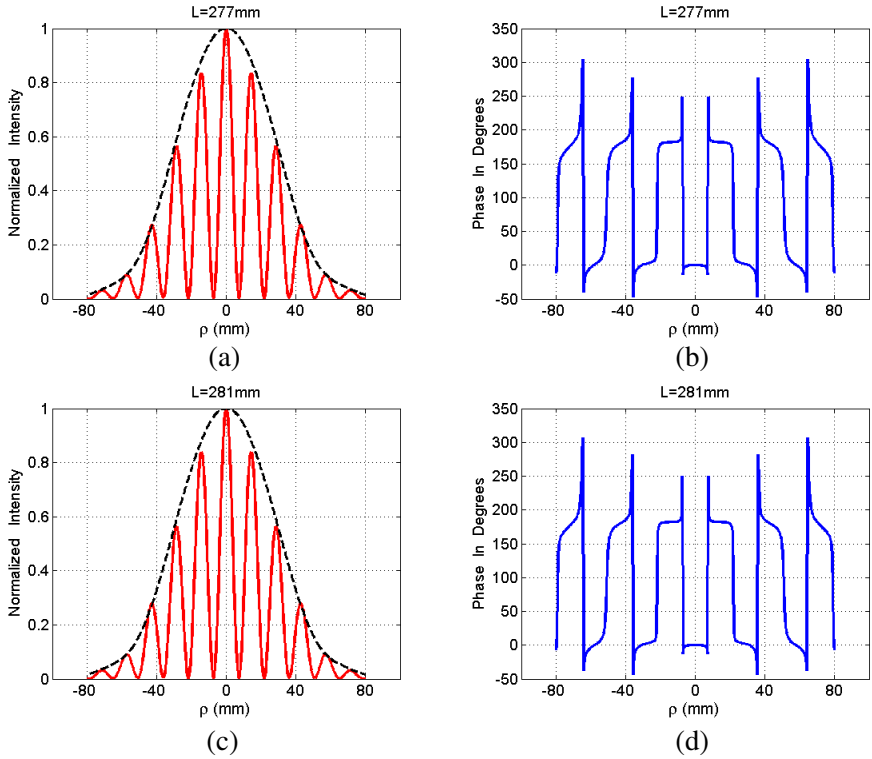

Figure 8. The effects of cavity length errors on the output modes. The intensity and phase distributions of the fundamental mode for (a), (b) $L = 277\,\text{mm}$ and (c), (d) $L = 281\,\text{mm}$.

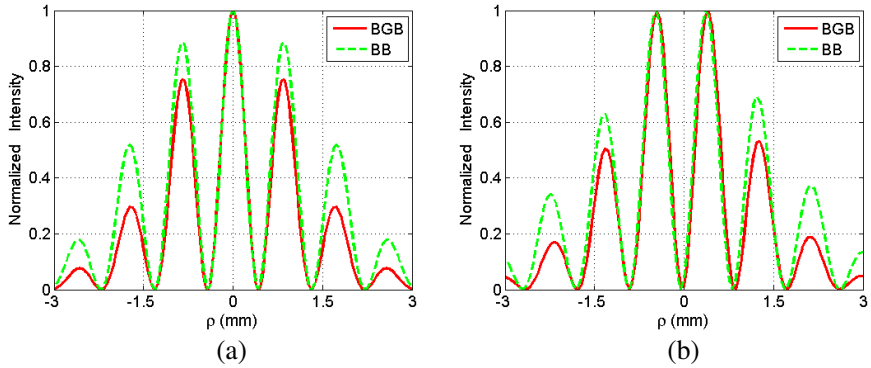

Figure 9. The transverse intensities of the fundamental and high-order modes for QOBGR and QOBR. (a) Fundamental modes, and (b) high-order modes, solid line (—) denotes Bessel-Gauss beam and dash line (----) represents Bessel beam.

the central axis z of the cavity, Bessel and Bessel-Gauss beams, whether dominate mode or high-order mode, have the same zero position and ring width. However, the extreme values of Bessel-Gauss beams are smaller than those of Bessel beams at the corresponding positions. The power losses of fundamental and high-order Bessel-Gauss modes are $\delta_0 = 1.38\%$ and $\delta_1 = 3.04\%$, respectively. But for the Bessel beam, $\delta_0 = 5.48\%$ and $\delta_1 = 9.31\%$. Thus a conclusion can be drawn that the power loss of QOBGR is much lower than that of QOBR, due to the convergence property of concave mirror in the cavity of QOBGR.

5. SUMMARY

A detailed analysis of the resonating modes in the QOBGR, constructed by the reflective axicon and the concave-spherical mirror, has been presented. Numerical simulations demonstrate that the designed QOBGR can sustain well, not only zero-order but also high-order, Bessel-Gauss like modes. Tolerance analysis is carried out provided that there exist the aperture errors, conical angle errors or cavity length errors, respectively. And analysis of the results confirm that in the distorted resonator the Bessel-Gauss mode is still supported approvingly. Finally, we compare the resonating modes between QOBR and QOBGR at SubMM-wavelengths. The Bessel-Gauss beam generated from the designed QOBGR have many promising applications in the MM- and SubMM-wavelength range, such as power transfer [26], millimeter wave imaging [27–29] and medium parameter measurement [30]. These applications are being studied at present.

ACKNOWLEDGMENT

This work is supported by State Key Lab of Millimeter Waves (No. K201307), and NSFC under grant 60921063.

REFERENCES

1. Durnin, J., "Exact solutions for nondiffracting beams. I. The scalar theory," *J. Opt. Soc. Am. A*, Vol. 4, No. 4, 651–654, 1987.
2. Durnin, J., J. J. Miceli, Jr., and J. H. Eberly, "Diffraction-free beams," *Phys. Rev. Lett.*, Vol. 58, No. 15, 1499–1501, 1987.
3. Monk, S., J. Arlt, D. A. Robertson, et al., "The generation of Bessel beams at millimetre-wave frequencies by use of an axicon," *Opt. Commun.*, Vol. 170, 213–215, 1999.
4. Gori, F., G. Guattari, and C. Padovani, "Bessel-Gauss beams," *Opt. Commun.*, Vol. 64, No. 6, 491–495, 1987.

5. Bagini, V., F. Frezza, M. Santarsiero, G. Schettini, and G. Schirripa Spagnolo, "Generalized Bessel-Gauss beams," *J. of Modern Optics*, Vol. 43, No. 6, 1155–1166, 1996.
6. Wu, F., Y. Chen, and D. Guo, "Nanosecond pulsed Bessel-Gauss beam generated directly from a Nd:YAG axicon-based resonator," *Appl. Opt.*, Vol. 46, No. 22, 4943–4947, 2007.
7. Elijah, Y. S. Y. and J. R. S. Colin, "Tight focusing of radially polarized Gaussian and Bessel-Gauss beams," *Opt. Lett.*, Vol. 32, No. 23, 3417–3419, 2007.
8. Grunwald, R, M. Bock, V. Kebbel, et al., "Ultrashort-pulsed truncated polychromatic Bessel-Gauss beams," *Opt. Express*, Vol. 16, No. 2, 1077–1089, 2008.
9. Winnerl, S., B. Zimmermann, F. Peter, H. Schneider, and M. Helm, "Terahertz Bessel-Gauss beams of radial and azimuthal polarization from microstructured photoconductive antennas," *Opt. Express*, Vol. 17, No. 3, 1571–1576, 2009.
10. Sabaeiana, M. and H. Nadgarana, "Bessel-Gauss beams: Investigations of thermal effects on their generation," *Optics Commun.*, Vol. 281, No. 4, 672–678, 2008.
11. Yu, Y. Z. and W. B. Dou, "Generation of pseudo-Bessel beams at THz frequencies by use of binary axicons." *Opt. Express*, Vol. 17, No. 2, 888–893, 2009.
12. Pääkkönen, P. and J. Turunen, "Resonators with Bessel-Gauss modes," *Opt. Commun.*, Vol. 156, No. 4–6, 359–366, 1998.
13. Rogel-Salazar, J., G. H. C. New, and S. Chávez-Cerda, "Bessel-Gauss beam optical resonator," *Opt. Commun.*, Vol. 190, No. 1–6, 117–122, 2001.
14. Gutiérrez-Vega, J. C., R. Rodríguez-Masegosa, and S. Chávez-Cerda, "Bessel-Gauss resonator with spherical output mirror: Geometrical and wave-optics analysis," *J. Opt. Soc. Am. A*, Vol. 20, No. 11, 2113–2122, 2003.
15. Ling, D. X., J. C. Li, and J. R. Chen, "Analysis of eigenfields in the axicon-based Bessel-Gauss resonator by the transfer-matrix method," *J. Opt. Soc. Am. A*, Vol. 23, No. 4, 912–918, 2006.
16. Litvina, I. A. and A. Forbes, "Bessel-Gauss resonator with internal amplitude filter," *Opt. Commun.*, Vol. 281, No. 9, 2385–2392, 2008.
17. Yu, Y. Z., and W. B. Dou, "Quasi-optical Bessel resonator," *Progress In Electromagnetics Research*, Vol. 93, 205–219, 2009.
18. Anatol, N. K., E. G. Katranji, and A. A. Ryzhevich, "Axicon-based Bessel resonator: Analytical description and experiment,"

J. Opt. Soc. Am. A, Vol. 18, No. 8, 1986–1992, 2001.

19. Mishra, M. and W. P. Hong, "Investigation on propagation characteristics of super-Gaussian beam in highly non-local medium," *Progress In Electromagnetics Research B*, No. 31, 175–188, 2011.
20. Sun, X. M., H. H. Wang, and H. Y. Zhang, "Scattering of Gaussian beam by a spheroidal particle," *Progress In Electromagnetics Research*, Vol. 128, 539–555, 2012.
21. Tao, R., L. Si, Y. Ma, P. Zhou, and Z. Liu, "Relay propagation of partially coherent cosh-Gaussian beams in non-Kolmogorov turbulence," *Progress In Electromagnetics Research*, 131, 495–515, 2012.
22. Tsangaris, C. L., G. H. C. New, and J. Rogel-Salazar, "Unstable Bessel beam resonator," *Optics Commun.*, Vol. 223, No. 4–6, 233–238, 2003.
23. Hernández-Aranda, R. I., S. Chávez-Cerda, and J. C. Gutiérrez-Vega, "Theory of the unstable Bessel resonator," *J. Opt. Soc. Am. A*, Vol. 22, No. 9, 1909–1917, 2005.
24. Fox, A. G. and T. Li, "Resonant modes in a maser interferometer," *Bell Syst. Tech. J.*, Vol. 40, 453–488, 1961.
25. Stratton, J. A., *Electromagnetic Theory*, McGraw-Hill, New York, 1941.
26. Jang, B.-J., S. Lee, and H. Yoon, "HF-band wireless power transfer system: Concept, issues, and design," *Progress In Electromagnetics Research*, V ol. 124, 211–231, 2012.
27. Zhou, Y., "Microwave imaging based on wideband range profiles," *Progress In Electromagnetics Research Letters*, Vol. 19, 57–65, 2010.
28. Tan, W. X., W. Hong, Y. P. Wang, and Y. R. Wu, "A novel spherical-wave three-dimensional imaging algorithm for microwave cylindrical scanning geometries," *Progress In Electromagnetics Research*, Vol. 111, 43–70, 2011.
29. An, D.-X., Z.-M. Zhou, X.-T. Huang, and T. Jin, "A novel imaging approach for high resolution squinted spotlight SAR based on the deramping-based technique and azimuth NLCS principle," *Progress In Electromagnetics Research*, Vol. 123, 485–508, 2012.
30. Xu, S., L. Yang, L. Huang, and H. S. Chen, "Experimental measurement method to determine the permittivity of extra thin materials using resonant metamaterials," *Progress In Electromagnetics Research*, Vol. 120, 327–337, 2012.